

The Effect of Laser Scanning Speed on Microstructure and Performance of Cr₃C₂-NiCr Cermet Fabricated by in-situ Laser Cladding

Deyuan LOU¹, Shaokun YANG¹, Sheng MEI¹, Qing LIU¹, Jian CHENG¹, Qibiao YANG¹, Dun LIU^{1*}, Chunlin HE²

¹ Laser Group, Department of Mechanical Engineering, Hubei University of Technology, Wuhan 430068, P. R. China

² Liaoning Provincial Key Lab of Advanced Materials, Shenyang University, Shenyang 110044, P. R. China

crossref <http://dx.doi.org/10.5755/j02.ms.23557>

Received 12 June 2019; accepted 31 October 2019

To explore the effect of laser scanning speed on the microstructure and performance of Cr₃C₂-NiCr cermet layers fabricated by in-situ laser cladding, Cr₃C₂-NiCr cermet layers were laser cladded from Ni/Cr/Graphite (25:65:10 wt.%) elemental powder mixtures. The microstructures of the laser cladded cermet layers and the formation mechanism were investigated. In addition, the effect of laser scanning speed on the microstructure, friction and corrosion performance of the Cr₃C₂-NiCr cermet layers was studied. The results indicated that the in-situ laser cladded Cr₃C₂-NiCr cermet layers were composed of NiCr binder and Cr₃C₂. The laser scanning speed had a significant influence on the carbide content, composition and size. Furthermore, it affected the in-situ laser cladded cermet layer's hardness and wear resistance. The corrosion resistance of the in-situ laser cladded cermet layer was superior to that of laser cladded nickel-based alloy and was improved with decreasing laser scanning speed.

Keywords: laser cladding, scanning speed, Cr₃C₂-NiCr, microstructure, corrosion.

1. INTRODUCTION

Cermets combine the hardness, oxidation resistance and high melting temperature of ceramic particles with the ductility, toughness and high thermal conductivity of metals; thus, they are ideal for use in high-temperature applications [1–3]. Nickel-based superalloys are characterized by high-temperature oxidation and corrosion resistance. In addition, the tribological properties of a metal applied by laser processing may be improved by introducing ceramic particles into a filler material.

The Cr₃C₂ particles used as additives for the reinforcement of MMC (Metal Matrix Composites) in laser processing usually decompose to M₇C₃, M₂₃C₆ and other carbides before solidification [4, 5]. Because the melting point and hardness of Cr₇C₃ and Cr₂₃C₆ are both lower than that of Cr₃C₂, the wear resistance of laser processed Cr₇C₃ MMC is inferior to that of Cr₃C₂ in high wear resistance applications [6–10]. Some work has been done on in-situ laser processing of Cr₃C₂-NiCr MMC, and the results have indicated that the ratios of the starting C/Cr/Ni elemental powder mixtures affect the phase of the in-situ laser processed Cr₃C₂-NiCr MMC [11, 12]. As the C/Cr ratio or C content is increased in the elemental powder starting material, the compositions and volume percent of carbides, and the properties of the in-situ laser processed cermet, vary considerably.

In addition, there are many parameters that affect the microstructures and performance of laser processed composites [13–16]; the laser specific energy (P/dv, where P is power, d is the laser spot diameter, and v is the scanning speed of the laser beam) is usually the most

important parameter influencing material and laser interactions [16]. In the present study, in-situ laser cladding from C/Cr/Ni elemental powders was used to fabricate Cr₃C₂-NiCr cermet layers, and the effect of laser parameters on the composition and properties of the processed Cr₃C₂-NiCr cermet layers was determined. It has been found that when the laser power and spot size are fixed, the laser scanning speed is of the greatest importance. Thus, the effect of laser scanning speed on in-situ cladded Cr₃C₂-NiCr single tracks will be discussed first, followed by the effect of laser scanning speed on the microstructures of in-situ laser cladded Cr₃C₂-NiCr cermet layers. Finally, the influence of scanning speed on the friction performance and corrosion resistance of in-situ laser cladded Cr₃C₂-NiCr cermet layers will be discussed.

2. MATERIALS AND METHODS

2.1. Materials

The powder mixtures were prepared from high-purity elemental powders of Cr, Ni, and graphitic carbon. These are summarized in Table 1, along with the purity and size of the powders used. The substrate used for laser processing was steel 45# (GB/T 699-1999), and the composition (wt.%) was: 0.45 C, 0.26 Ni, 0.68 Mn, 0.008 P, 0.013 S, and the balance Fe. These powders were measured and mixed to a nominal composition of 65 wt.% Cr, 25 wt.% Ni, and 10 wt.% C. The elemental powders are the same to the previous work [12] and has been shown in Fig. 1.

* Corresponding author. Tel.: +86-27-59750418; fax: +86-27-59750417.
E-mail address: Dun.liu@hbut.edu.cn (D. Liu)

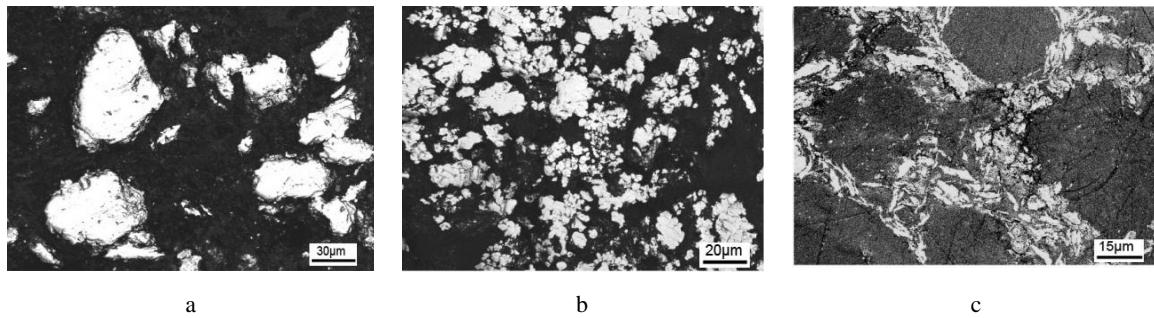


Fig. 1. Optical images of the element powders used in laser processing: a–Cr; b–Ni; c–graphite (Powder samples were prepared with polymer binder, the light parts of Fig. 1 a, b–are metals whereas black part in Fig. 1 c is graphite) [12]

Table 1. Chemical composition, particle size and purity of the powders used in in-situ laser cladding

	Ni	Cr	Graphite
Sample, wt.%	25.00	65.00	10.00
Particle size, μm	10–50	10–50	30–50
Purity, wt.%	99.9	99.9	99.85

2.2. In-situ laser cladding processing

The powders were uniformly preplaced on an 8 mm thick 45# steel substrate with the height control set at 1.2 mm. In-situ laser cladding was carried out in air using a DL-HL-T type 5 kW CO₂ CW laser and keeping the following parameters constant for all samples: laser power 3 kW and laser spot diameter 3.5 mm. Laser scanning speed is a practical technical parameter, although the laser impact on material depends on laser input energy densities. CNC (Computerized Numerical Control) platform was utilized to make uniform move in x-y directions. For single track cladding, the scanning speeds were 10 mm/s, 15 mm/s, 20 mm/s, 25 mm/s and 30 mm/s, respectively. For multi-track cladding (1 mm–2 mm thick), the routes were s-shaped, the overlaps were all 30 %, and the scanning speeds were 10 mm/s, 20 mm/s, 30 mm/s and 40 mm/s, respectively.

2.3. Characterization of microstructures

Specimens for X-ray diffraction (XRD) were prepared via polishing the top of the cermet layer, and XRD (X'Pert Pro MPD-Pw3040/60) studies were carried out using Cu K α radiation to analyze the constituent phases. The cross sections (perpendicular to the laser scanning direction) of the layers were investigated using a laser confocal microscopy (Olympus-ols3100), scanning electron microscopy (SEM, SuperSean55-550) and energy dispersive X-ray analysis (EDX). Image analysis was also used to analyze quantitatively the surface fractions of the graphite.

2.4. Microhardness, wear and corrosion tests

The microhardness test was carried out using a 401MVD Digital Vickers Hardness tester on the cross section of the samples; the load was 0.3 kg. Wear tests were performed using a MFT-4000 ball-on-disk reciprocating tribometer (Lanzhou Institute of Chemistry Physics) at an ambient temperature of approximately 25 °C and a relative humidity of 40 %. Si₃N₄ balls with a

diameter of 4 mm were used as the counterparts. The sliding speed was 100 mm/min with a load of 0.3 kg and a sliding stroke length of 5 mm.

Electrochemical measurements were made at room temperature in a three-electrode cell containing a 0.2 M H₂SO₄ aqueous solution. The instruments used were a Solartron1250 frequency response analyzer and a model EG&G273 potentiostat. A saturated calomel electrode (SCE) was used as the reference electrode, and the counter electrode was graphite. Potentiodynamic polarization tests were carried out at a scanning rate of 0.332 mV/s. Electrochemical Impedance Spectroscopy (EIS) was measured by perturbing the open circuit potential of the specimens with a 10 mV ac signal with a frequency decreasing from 105 Hz to 0.01 Hz.

3. RESULTS AND DISCUSSION

3.1. Effect of laser scanning speed on the in-situ cladding of Cr₃C₂-NiCr single tracks

3.1.1. Effect of laser scanning speed on the shape of in-situ cladded Cr₃C₂-NiCr single tracks

The cross section of the laser cladded single track is depicted in the schematic diagram in Fig. 2. As shown in Fig. 2, substrate is melted and the height of the laser cladded single track is h ; the melting depth of the substrate is h_1 , the width of the cladded track is W , the width to height ratio of the cladded track is W/h , the contact angle of the cladded track is θ and the maximum depth of the Heat Affected Zone (HAZ) is H , the geometry dilution ratio is $h_1/(h + h_1)$. Laser cladding parameters determine the dilution ratio and the shape of single tracks generally.

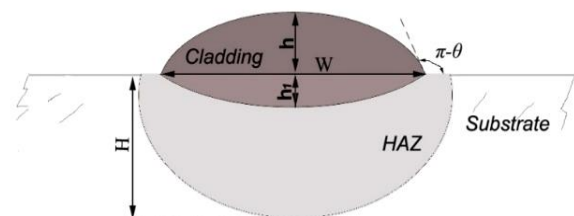


Fig. 2. Schematic diagram of a cross section of in-situ laser cladded Cr₃C₂-NiCr cermet single track

According to the definition of specific energy ($E = P/dv$) [17], when the laser power, spot size and

powder composition are fixed, scanning speed is the primary determinant of the temperature distribution in the laser melt and of the resulting microstructures. The shape parameters (contact angle θ , dilution rate η , the maximum cladding height h , and the maximum thickness of the heat affected zone H) of the laser cladded single tracks are shown in Fig. 3 the curves in dashed lines are fitted linearly. The figure demonstrates that the laser scanning speed v has a decisive influence on the cladded tracks' shape parameters. Laser energy is enough to melt powder, when laser scanning speed increase, less radiate energy goes through the powder into substrate and make less melted powder move (diffuse, spread) to the substrate position. In general, h and H increase with the increasing v , but η and θ decrease with increasing v .

3.1.2. Effect of laser scanning speed on the bonding zone of in-situ laser cladded Cr₃C₂-NiCr single tracks

Fig. 4 shows the microstructures near the binding region of in-situ laser cladded single tracks generated at different scanning speeds. It is apparent that the binding zone (planar zone, the interface was indicated by red dash lines) becomes smoother as the laser scanning speed decreases. As the laser scanning speed increases, the cladding of melt droplets onto the substrate becomes more unbalanced. Further, the interaction between cladding material and the substrate is enhanced, resulting in the binding zone grow thinner and the formation of dendrites that are finer and shorter [18–20]. As the laser beam

irradiates the C/Cr/Ni powder, the Ni and Cr powders melt first and the NiCr melt comes in contact with the 45# steel substrate. The NiCr and substrate diffuse into each other, so that the concentrations of Cr and Ni in the substrate increase.

As determined experimentally, the spacing (λ_{SDAS}) between the secondary dendrite arm spacing and the solidification cooling rate may be expressed as [21–23]:

$$\lambda_{SDAS}(\mu\text{m}) = \begin{cases} (169.1 - 720.9 C_c) C_R^{-0.4935} & (0 < C_c \leq 0.15), \\ 143.9 C_R^{-0.3616} C_c^{(0.5501-1.996 C_c)} & (C_c > 0.15) \end{cases}, \quad (1)$$

where C_c is the carbon content (wt.%), and C_R is cooling rate. The solidification cooling rate can be estimated from different laser scanning speeds. The carbon content at the interface can be approximated as 1 wt.%, and the scanning speeds corresponding to the estimated cooling rates are shown in Table 2. From the table, it is apparent that the cooling rate of the cladded material varies with the laser scanning speed. Therefore, the laser scanning speed directly causes changes in the size of the solidified structures near the bonding zone.

Table 2. Solidification rate of the bonding zone in in-situ laser cladding correlates with scanning speed

v, mm/s	10	15	20	25	30
CR, K/s	9.3×10^4	2.2×10^5	4.2×10^5	5.5×10^5	1.2×10^6

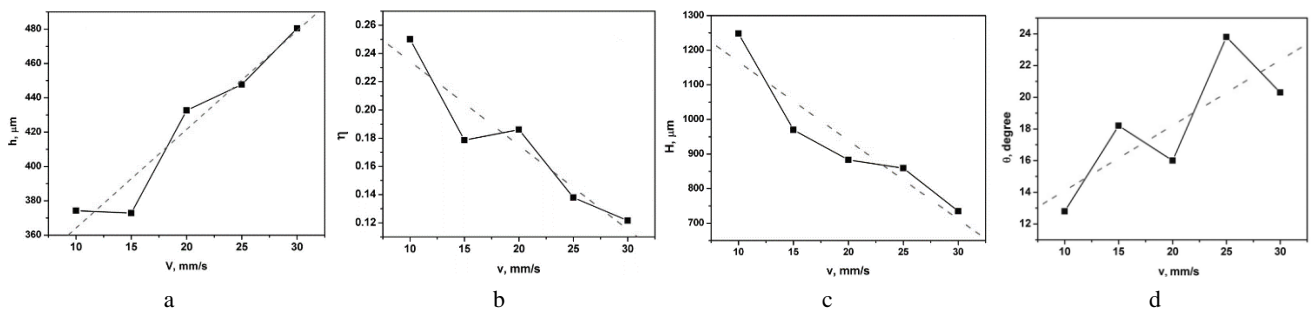


Fig. 3. Relationship curves between laser scanning speed and the characteristic parameters of laser cladded Cr₃C₂-NiCr single track: a – h_1 - v ; b – η - v ; c – H - v ; d – θ - v

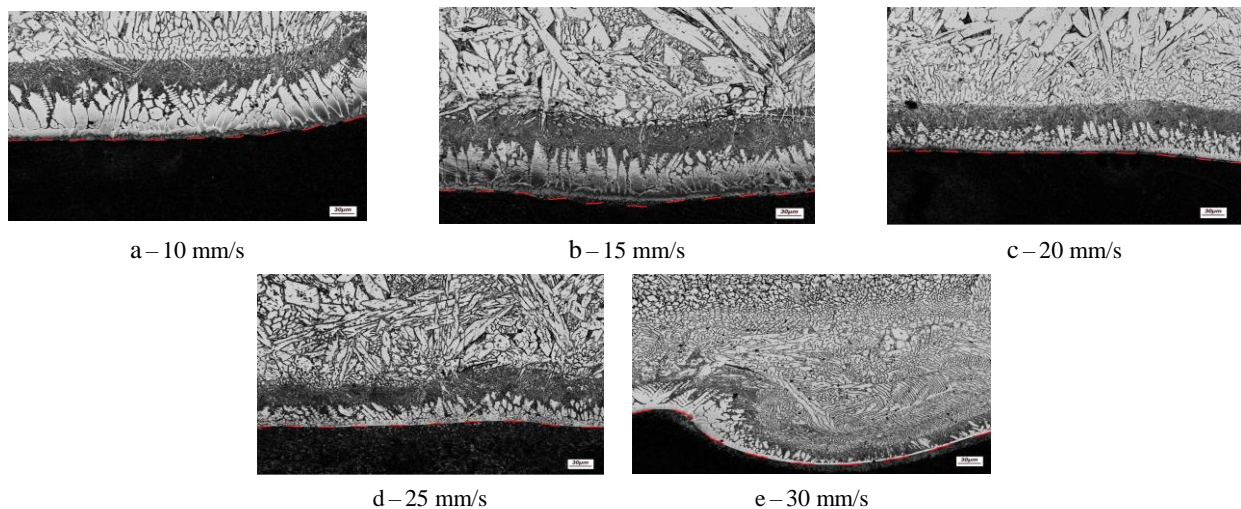


Fig. 4. Effect of laser scanning speed on the bonding zones of in-situ laser cladded Cr₃C₂-NiCr

3.2. Effect of laser scanning speed on the microstructure of in-situ laser clad Cr_3C_2 -NiCr cermet layers

3.2.1. Phase analysis of in-situ laser clad Cr_3C_2 -NiCr cermet layers

From the curves, it is clear that Ni-based solid solution (NiCr) and carbide ($\text{Cr}_3\text{C}_2/\text{Cr}_7\text{C}_3$) are the main phase in each layer. Using a method previously employed to calculate the volume content of $\text{Cr}_3\text{C}_2/\text{Cr}_7\text{C}_3$ in composites [24, 25], the volume content of Cr_3C_2 and Cr_7C_3 is estimated to be more than 74 %. Furthermore, the scanning speed has a great influence on the cermet composition: with an increase in scanning speed, the diffraction peak intensity ratio between NiCr and carbide decreases, indicating that the content of carbide increases while the content of NiCr decreases. Moreover, the type of carbide clad is also affected by laser scanning speed. By comparing the diffraction peak intensities of Cr_3C_2 and Cr_7C_3 in Fig. 5, it can be observed that more Cr_3C_2 is generated as the laser scanning speed increases, while less Cr_7C_3 appears in the laser cladding layer.

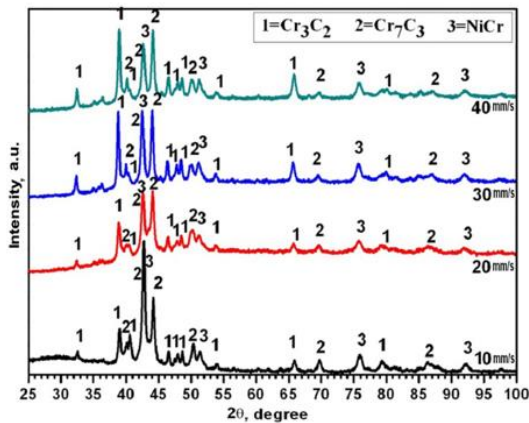


Fig. 5. XRD spectra of in-situ laser clad cermet layers formed at various scanning speeds

The reason for the cladding layer composition

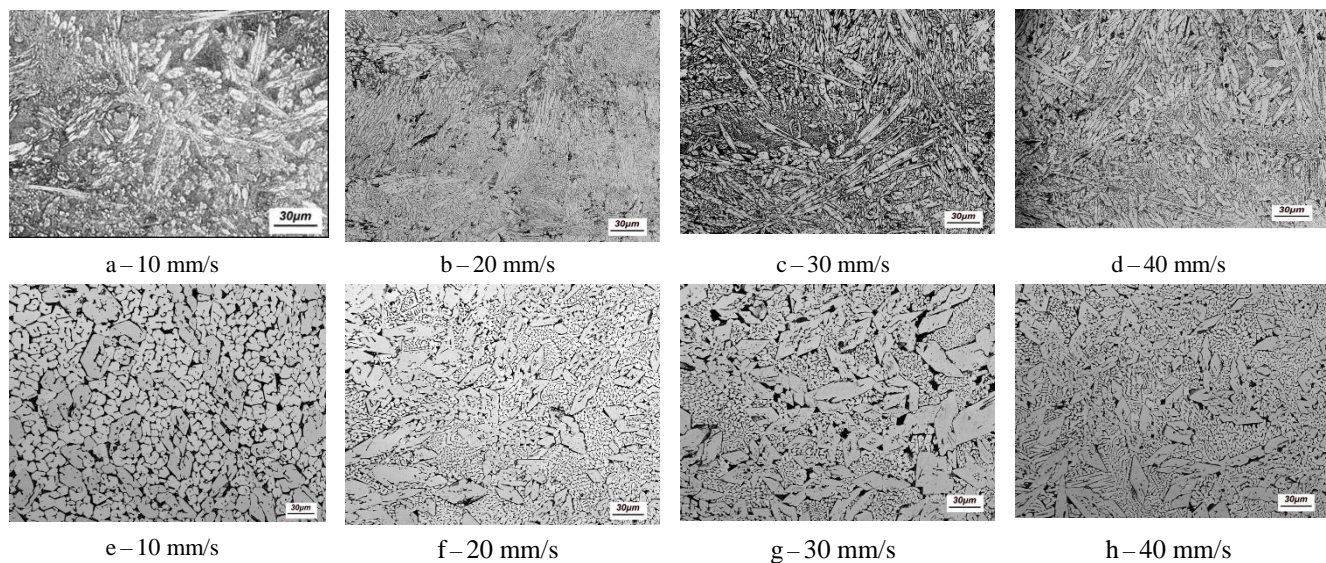


Fig. 6. Cross-section images of in-situ laser clad Cr_3C_2 -NiCr cermet with various scanning speed: (a), (b), (c) and (d) are longitudinal sections; (e), (f), (g) and (h) are transverse section

changing as a function of laser scanning speed is as follows: when the scanning speed becomes slower, the input energy density increases and the cooling rate declines, resulting in the solidification process being closer to equilibrium. Due to the formation enthalpy of Cr_7C_3 being less than that of Cr_3C_2 , it is easier to produce Cr_7C_3 at lower scanning speeds; conversely, it is easier to produce Cr_3C_2 at higher scanning speeds.

3.2.2. Microstructures of in-situ laser clad Cr_3C_2 -NiCr cermet layers

Fig. 6 shows images of longitudinal and transverse sections of laser clad Cr_3C_2 -NiCr cermet layers. The figure demonstrates that laser clad cermet layers are mainly composed of a binder phase and carbides. Furthermore, the size, distribution and morphology of the carbide are closely related to the scanning speed. With faster laser scans, the temperature distribution becomes more unstable, resulting in a more uneven distribution of carbides with reduced size, more carbide growing in the horizontal direction, and more elongated cross sections. By cross-section image analysis, it is apparent that the carbide area ratio varies with different laser scanning speed: the faster the speed, the higher the area fraction of carbides (Table 3). This is consistent with the XRD analysis results above.

Table 3. Area fractions of carbides in the in-situ laser clad Cr_3C_2 -NiCr cermet at different scanning speed

Scanning speed, mm/s	10	20	30	40
Area fraction of carbides, %	49.2	53.0	54.2	65.8

Fig. 7 shows SEM images and EDX spectra of laser clad Cr_3C_2 -NiCr cermet layers. It can be observed that a variety of shapes precipitate in the cermet, including hexagonal, square, strips and branched, etc. EDS analysis was carried on the different shapes (indicated as spots A, B, C, D in Fig. 8); together with the results of TEM analysis [11, 12], it can be concluded that the hexagonal precipitate is Cr_7C_3 (A), and the square precipitates are Cr_3C_2 (C).

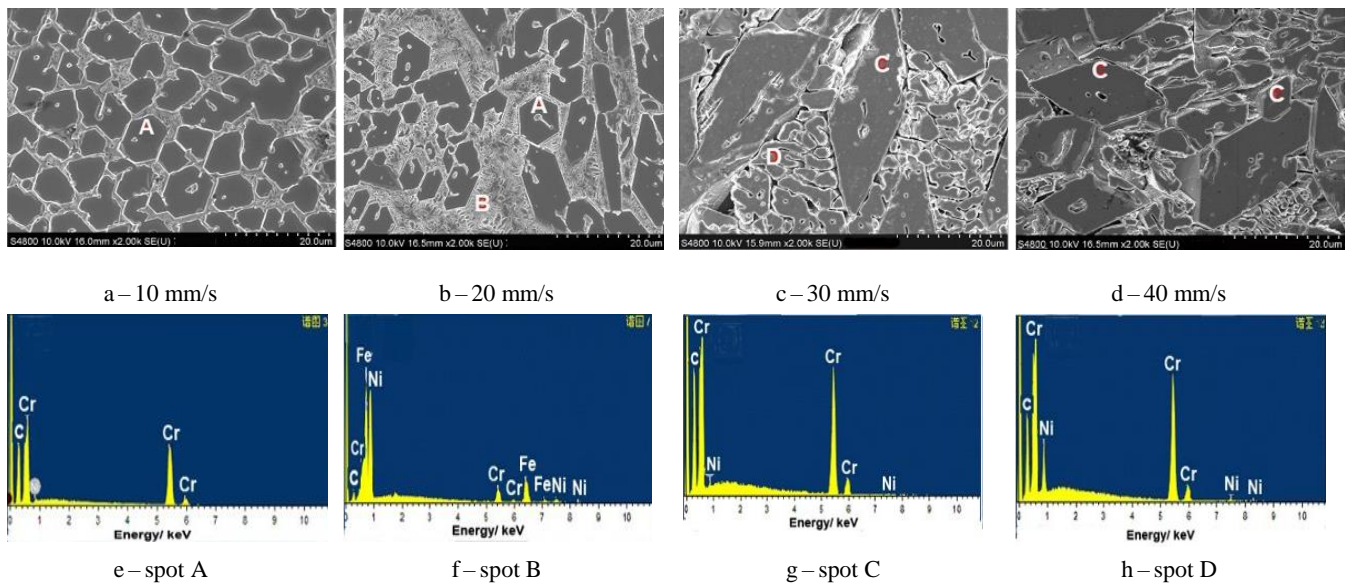


Fig. 7. SEM images and EDX spectra of in-situ laser clad $\text{Cr}_3\text{C}_2\text{-NiCr}$ cermet at different scanning speeds

However, the composition of the strip-shaped carbide was not determined, and it may be Cr_3C_2 or Cr_7C_3 . The binder between these carbides is eutectic carbide (B), composed of fine carbides and Ni austenite; some of the fine carbide grew coarser and aggregated to a size of several microns (D).

If the laser scanning speed reduced, the laser irradiation time on the same position increase (and thus the powder absorbs more energy density), the solidification time becomes longer and the average size (estimated from images) of the carbide increases. At the same time, when laser scanning speeds become slower, the melt cools more slowly and is closer to an equilibrium solidification process; thus, it is easy to generate Cr_7C_3 with low synthetic thermodynamic enthalpy. As a result, the carbide in the 10 mm/s sample grew in a hexagonal fashion.

3.3. Effect of scanning speed on the friction performance and corrosion resistance of laser clad $\text{Cr}_3\text{C}_2\text{-NiCr}$ cermet layers

Fig. 8 shows microhardness distributions of in-situ laser clad $\text{Cr}_3\text{C}_2\text{-NiCr}$ cermet layers fabricated at different scanning speeds. It can be observed that the cladding layer formed at the slowest speed afforded the lowest microhardness: only approximately $550 \text{ HV}_{0.3}$. However, the hardness distribution of the 10 mm/s sample was uniform, which was due to its uniform ceramic phase distribution, and the ceramic relatively same in size. As the laser scanning speed increased, the content of Cr_3C_2 was enhanced and the microhardness was improved, which results in the hardness improvement and slightly decline of the friction coefficient. However, while the microhardness increased with faster laser scans, the microhardness distribution became more non-uniform. The XRD results indicated that the 40 mm/s sample had the maximum Cr_3C_2 content. Among the three carbides, Cr_3C_2 , Cr_7C_3 and Cr_{23}C_6 , the microhardness of Cr_3C_2 is the highest, so the 40 mm/s sample had the highest hardness; in fact, its microhardness approached $1230 \text{ HV}_{0.3}$, or approximately 5.6 times that of the matrix hardness ($220 \text{ HV}_{0.3}$).

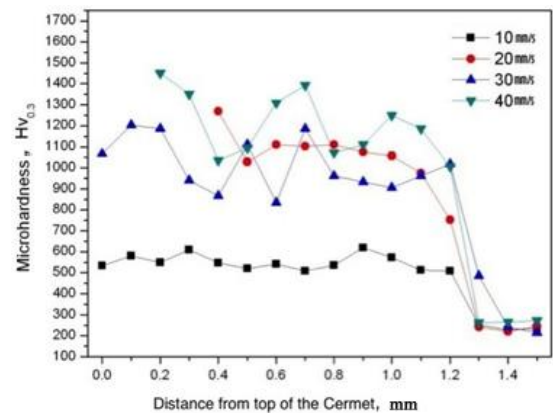


Fig. 8. Effect of laser scanning speed on the microhardness distributions of in-situ laser clad $\text{Cr}_3\text{C}_2\text{-NiCr}$ cermet

Fig. 9 illustrates the effect of scanning speed on the friction coefficient of laser clad $\text{Cr}_3\text{C}_2\text{-NiCr}$ cermet layers.

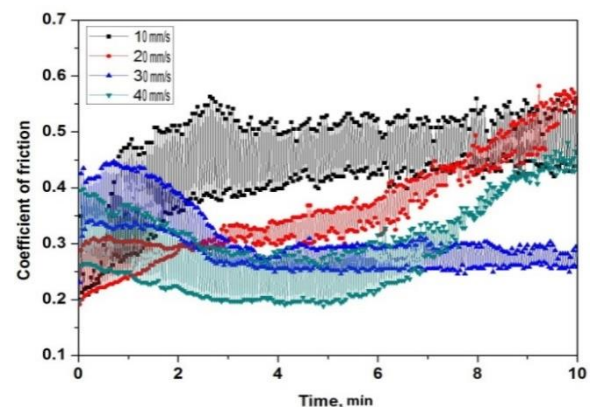


Fig. 9. Effect of scanning speed on the friction coefficient of in-situ laser clad $\text{Cr}_3\text{C}_2\text{-NiCr}$ cermet

It can be observed from the curves that the friction coefficient of every sample was large in the initial running-in stage; however, that of the 40 mm/s and 30 mm/s samples declined to stable values after two minutes of the

friction test. The friction coefficient of the 10 mm/s sample maintained a high fixed value throughout the test. After six minutes, the friction coefficients of the 20 mm/s and 40 mm/s samples began to increase slowly to a value as high as that of the 10 mm/s sample. Overall, the average friction coefficients were 0.46 for 10 mm/s, 0.32 for 20 mm/s, 0.27 for 30 mm/s and 0.24 for 40 mm/s; that is, the friction coefficient decreased with decreasing laser cladding scanning speed.

The above experiments demonstrate that as the scanning speed of in-situ laser cladding increases, the composition and content of the reinforcement phase of the cladding layer changes; specifically, the carbide content (especially Cr_3C_2) increases, and with it the cladded layer's hardness. This results in an increase in the resistance grindability of the in-situ laser cladded cermet layer.

In order to study the effect of laser scanning speed on the corrosion behavior of the in-situ laser cladded Cr_3C_2 -NiCr cermet samples, cyclic potentiodynamic polarization experiments were carried out in 3.5 % NaCl aqueous solution. Fig. 10 shows the potentiodynamic curves of the samples in 3.5 % NaCl aqueous solution. It is clear that all of these samples show nearly complete passivation. The values of the corrosion potential (E_{Corr}) and the corrosion current density (i_{Corr}) in 3.5 % NaCl aqueous solutions as a function of different laser scanning speeds are shown in Table 4.

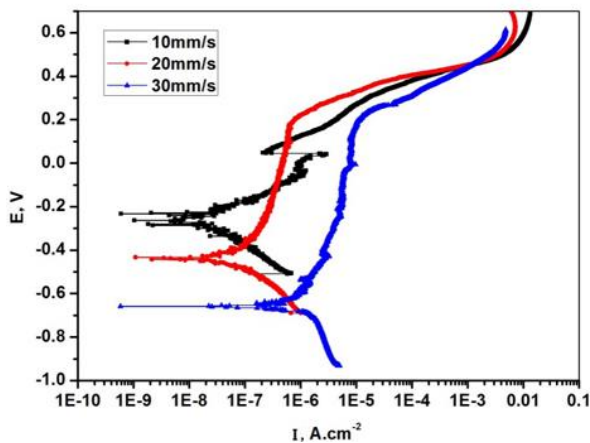


Fig. 10. Effect of scanning speed on the potentiodynamic curves of in-situ laser cladded Cr_3C_2 -NiCr cermet in 3.5 % NaCl aqueous solutions

Table 4. Corrosion potential and corrosion current density of in-situ laser cladding Cr_3C_2 -NiCr cermet at different scanning speeds

Sample scanning speed, mm/s	E_{Corr} , mV	i_{Corr} , $\text{A}\cdot\text{cm}^{-2}$
10	-271	1.8 E^{-8}
20	-465	3.7 E^{-8}
30	-653	4.7 E^{-7}

It is clear that the order of i_{Corr} is as follows: 30 mm/s > 20 mm/s > 10 mm/s, which indicates that the corrosion rate value increases with increasing laser scanning speed, and forward the optimum corrosion potential and corrosion current density are -271 mV and $1.8 \times 10^{-8} \text{ Acm}^{-2}$, respectively. Although the content of carbide grows and the galvanic corrosion tendency

weakens, but pitting corrosion and crevice corrosion increases due to the defects (microcracks/cavities) increase, as shown in Fig. 10.

At the same time, E_{Corr} declines when the laser scanning speed is increased. Thus, the corrosion resistance of in-situ cladded Cr_3C_2 -NiCr cermet layers in 3.5 % NaCl aqueous solution improves as the laser scanning speed is decreased. Based on the corrosion data for nickel-based alloy (Hastelloy-C22, laser cladded) in the same solution [26], it is evident that the corrosion resistance of in-situ laser cladded Cr_3C_2 -NiCr cermet layers is better than that of laser cladded Hastelloy-C22 layers in 3.5 % NaCl aqueous solution.

The standard electrode potentials of carbide in nickel based composite is higher than that of base alloy, thereby forms an electrochemical corrosion micro battery in the electrolyte. Furthermore, this effect is presumed to be strengthened with the increase of carbide content (only when the carbide content is less than 50 %), resulting in growth of corrosion rate in dilute sulfuric acid solution. So corrosion resistance of in-situ cladded Cr_3C_2 -NiCr cermet layers improves as the laser scanning speed decreases. From the morphology of the specimen after corrosion (Fig. 11), it can be seen that the most serious corrosion happens at the interfaces between carbide and matrix, graphite and matrix, respectively.

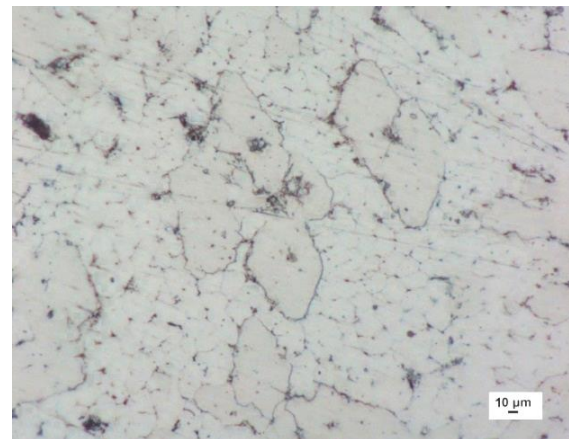


Fig. 11. Corrosion morphology of laser cladded Cr_3C_2 -NiCr cermet (scanning speed 30 mm/s) in 3.5% NaCl aqueous solution

4. CONCLUSIONS

Three major conclusions emerge from the present study. First, in-situ laser cladded Cr_3C_2 -NiCr cermet layers are composed of NiCr solid solution (binder) and carbides (Cr_3C_2 , Cr_7C_3). The laser scanning speed v has a significant influence on the carbide content. When v increases, the solidification rate of the laser melt pool increases, and the carbide size becomes smaller; moreover, the carbide content increases, the content of Cr_3C_2 increases, and the content of Cr_7C_3 is reduced. As v increases to greater than 30 mm/s, the dominant carbide becomes Cr_3C_2 .

Due to the variation of carbide composition, content and size distribution as a function of laser scanning speed v , the scanning speed affects in-situ laser cladded cermet layer hardness and wear resistance. As v increases, the microhardness of the Cr_3C_2 -NiCr cermet layer increases

and its wear resistance is enhanced. The in-situ laser clad Cr₃C₂-NiCr cermet layer hardness may approach 1230 HV_{0.3}. The minimum friction coefficient of the Cr₃C₂-NiCr cermet layer is 0.24, which is 0.52 times that of the maximum.

With regard to galvanic corrosion occurring between the carbide and the NiCr binder in 3.5% NaCl aqueous solution, the corrosion resistance of in-situ clad Cr₃C₂-NiCr cermet layers improves as v decreases. The corrosion resistance of the in-situ laser clad cermet layer is superior to that of laser clad nickel-based alloy; the optimum corrosion potential and corrosion current density are -271 mV and 1.8 × 10⁻⁸ Acm⁻², respectively.

Acknowledgments

This research was financially supported by Research Fund of Hubei Provincial Education Department (D20191405) and Open Fund of RAL of Northeastern University (2016001).

REFERENCES

1. **Wood, R.J.** Tribo-corrosion of Coatings: A Review *Journal of Physics D: Applied Physics* 40 2007: pp. 5502–5521. <https://doi.org/10.1088/0022-3727/40/18/S10>
2. **Bergmann, C.P., Vicenzi, J.** Protection against Erosive Wear Using Thermal Sprayed Cermet: A Review *Protection Against Erosive Wear Using Thermal Sprayed Cermet* 2011: pp. 315–326. https://doi.org/10.1007/978-3-642-21987-0_1
3. **Chang, C., Verdi, D., Garrido, M.A.** Micro-scale Mechanical Characterization of Inconel Cermet Coatings Deposited by Laser Cladding *Boletín de la Sociedad Española de Cerámica y Vidrio* 55 (4) 2016: pp. 136–142. <https://doi.org/10.1016/j.bsecev.2016.01.001>
4. **Lin, L., Li, G.L., Wang, H.D., Kang, J.J., Xu, Z.L., Wang, H.J.** Structure and Wear Behavior of NiCr–Cr₃C₂Coatings Sprayed by Supersonic Plasma Spraying and High Velocity Oxy-fuel Technologies *Applied Surface Science* 356 2015: pp. 383–390. <https://doi.org/10.1016/j.apsusc.2015.08.019>
5. **Gnanasekaran, S., Padmanaban, G., Balasubramanian, V., Kumar, H., Albert, S.K.** Laser Hardfacing of Colmonoy-5 (Ni-Cr-Si-B-C) Powder onto 316LN Austenitic Stainless Steel: Effect of Powder Feed Rate on Microstructure, Mechanical Properties and Tribological Behavior *Laser in Engineering* 42(4-6) 2019: pp. 283-302.
6. **Kathuria, Y.P.** Nd: YAG Laser Cladding of Cr₃C₂ and TiC Cermets *Surface and Coatings Technology* 140 (3) 2001: pp. 195–199. [https://doi.org/10.1016/s0257-8972\(01\)01046-5](https://doi.org/10.1016/s0257-8972(01)01046-5)
7. **Kaiming, W., Yulong, L., Hanguang, F., Yongping, L., Zhenqing, S., Pengfei, M.** A Study of Laser Cladding NiCrBSi/Mo Composite Coatings *Surface Engineering* 34 (4) 2018: pp. 267–275. <https://doi.org/10.1080/02670844.2016.1259096>
8. **John, C.B.** The Direct Laser Deposition of AISI316 Stainless Steel and Cr₃C₂ Powder *Journal of Materials Processing Technology* 209 (11) 2009: pp. 5229–5238. <https://doi.org/10.1016/j.jmatprotec.2009.03.010>
9. **Liu, X.B., Gu, Y.J.** Plasma Jet Clad γ /Cr₇C₃Composite Coating on Steel *Materials Letters* 60 2006: pp. 577–580. <https://doi.org/10.1016/j.matlet.2005.09.041>
10. **Jeyaprakash, N., Yang, CH., Duraiselvam, M., Prabu, G.** Microstructure and Tribological Evolution during Laser Alloying WC-12 % Co and Cr₃C₂–25 % NiCr Powders on Nodular Iron Surface *Results in Physics* 12 2019: pp. 1610–1620. <https://doi.org/10.1016/j.rinp.2019.01.069>
11. **Lou, D.Y., He, C.L., Shang, S., Liu, C.S., Cai, Q.K.** Microstructure and Performances of Graphite Scattered Cr₃C₂-NiCr Composites Prepared by Laser Processing *Materials Letters* 93 2013: pp. 304–307. <https://doi.org/10.1016/j.matlet.2012.11.113>
12. **Lou, D.Y., Liu, D., He, C.L., Bennett, P., Chen, L., Yang, Q.B., Fearon, E., Dearden, F.** Effect of Cr/C Ratio on Microstructure and Corrosion Performance of Cr₃C₂-NiCr Composite Fabricated by Laser Processing *Journal of Materials Engineering and Performance* 25 (1) 2016: pp. 312–319. <https://doi.org/10.1007/s11665-015-1843-0>
13. **Sun, Y.W., Hao, M.Z.** Statistical Analysis and Optimization of Process Parameters in Ti6Al4V Laser Cladding Using Nd: YAG Laser *Optics and Lasers in Engineering* 50 (7) 2012: pp. 985–995. <https://doi.org/10.1016/j.optlaseng.2012.01.018>
14. **Lou, DY., Cao, J.F., Huang, Y., Lin, C.H., He, C.L., Bennett, P., Liu, D.** Effect of Ball Milling on The Microstructure and Performances of Laser Clad Forming Cr3C2-NiCr Composites *Rapid Prototyping Journal* 25 (3) 2019: pp. 448–453. <https://doi.org/10.1108/RPJ-08-2017-0166>
15. **Marzban, J., Ghaseminejad, P., Ahmadzadeh, M.H., Teimouri, R.** Experimental Investigation and Statistical Optimization of Laser Surface Cladding Parameters *TheInternational Journal of Advanced Manufacturing Technology* 76 (5–8) 2015: pp. 1163–1172. <https://doi.org/10.1007/s00170-014-6338-x>
16. **Emamian, A., Corbin, S.F., Khajepour, A.** Effect of Laser Cladding Process Parameters on Clad Quality and in-situ Formed Microstructure of Fe-TiC Composite Coatings *Surface and Coating Technology* 205 (7) 2010: pp. 2007–2015. <https://doi.org/10.1016/j.surfcoat.2010.08.087>
17. **Steen, W., Watkins, K.G., Mazumder, J.** Laser Material Processing *Springer Press* 2010: pp. 131–198. <https://doi.org/10.1007/978-1-84996-062-5>
18. **Lin, X.** Evolution and Selection of Micro Substructure in Solidification, *Ph D Thesis, China*. 2000: pp. 3–29.
19. **Huang, Y.J., Zeng, X.Y., Hu, Q.W., Zhou, S.F.** Study on Interface Characteristics in Laser Induction Hybrid Cladding *Applied Laser* 27 (6) 2007: pp. 465–469. <https://doi.org/10.3969/j.issn.1000-372X.2007.06.006>
20. **Wang, S., Zhang, S., Zhang, CH., Wu, CL., Chen, J., Shahzad, M.B.** Effect of Cr3C2 Content on 316L Stainless Steel Fabricated by Laser Melting Deposition *Vacuum* 147 2018: pp. 92–98. <https://doi.org/10.1016/j.vacuum.2017.10.027>
21. **Chen, Y., Wang, H.M.** Liquid/Solid Interface Structure and Growth Mechanism of the Carbidunder Non-equilibrium Solidification Conditions *Acta Metalurgical Sinica* 3 2003: pp. 254–258.
22. **Wang, S., Zhang, S., Zhang, CH., Wu, CL., Chen, J., Shahzad, M.B.** Effect of Cr3C2 Content on 316L Stainless Steel Fabricated by Laser Melting Deposition *Vacuum* 147 2018: pp. 92–98.
23. **Won, Y.M., Thomas, B.G.** Simple Model of Micro Segregation during Solidification of Steels *Metallurgical*

and *Materials Transactions A* 32 2001: pp. 1755 – 1760.
<https://doi.org/10.1007/s11661-001-0152-4>

24. **Zhou, Y.** *Analysis Methods in Material Science* China Machine Press 2017: pp. 47 – 54.
25. **Val'chuk, V.P., Zmienko, D.S., Kolesov, V.V., Bokova-Sirosh, S.N., Dolotova, T.S.** Novel Ni-Cr-C Alloys with Chromium Carbide Whiskers *Materials Chemistry and Physics* 213 2018: pp. 191 – 197.

<https://doi.org/10.1016/j.matchemphys.2018.04.034>

26. **Wang, Q.Y., Zhang, Y.F., Bai, S.L., Liu, Z.D.** Microstructures Mechanical Properties and Corrosion Resistance of Hastelloy C22 Coating Produced by Laser Cladding *Journal of Alloys and Compounds* 553 2013: pp. 253 – 258.
<https://doi.org/10.1016/j.jallcom.2012.10.193>



© Lou et al. 2021 Open Access This article is distributed under the terms of the Creative Commons Attribution 4.0 International License (<http://creativecommons.org/licenses/by/4.0/>), which permits unrestricted use, distribution, and reproduction in any medium, provided you give appropriate credit to the original author(s) and the source, provide a link to the Creative Commons license, and indicate if changes were made.